Identifying Tissue-Specific Signal Variation in MALDI Mass Spectrometric Imaging by Use of an Internal Standard

David A. Pirman,[†] András Kiss,[‡,§] Ron M. A. Heeren,[‡,§] and Richard A. Yost*[,†]

[†]Department of Chemistry, University of Florida, Gainesville, Florida, 32607, United States

[‡]FOM Institute for Atomic and Molecular Physics (AMOLF), Science Park 104, 1098 XG Amsterdam, The Netherlands

[§]Netherlands Proteomic Center, Utrecht, The Netherlands

ABSTRACT: Generating analyte-specific distribution maps of compounds in a tissue sample by matrix-assisted laser desorption/ionization (MALDI) mass spectrometric imaging (MSI) has become a useful tool in numerous areas across the biological sciences. Direct analysis of the tissue sample provides MS images of an analyte's distribution with minimal sample pretreatment. The technique, however, suffers from the inability to account for tissue-specific variations in ion signal. The variation in the makeup of different tissue types can result in significant differences in analyte extraction, cocrystallization, and ionization across a sample. In this study, a deuterated internal standard was used to account for these signal variations. Initial experiments were performed using pure standards and optimal cutting temperature compound (OCT) to generate known areas of ion suppression. By monitoring the analyte-to-internal-standard ratio, differences in ion signal were taken into account, resulting in images that better represented the analyte concentration. These experiments were then replicated using multiple tissue types in which the analyte's MS signal was monitored. In certain tissues, including liver and kidney, the analyte signal was attenuated by up to 90%; however, when the analyte-to-internal-standard ratio was monitored, these differences were taken into account. These experiments further exemplify the need for an internal standard in the MSI workflow.

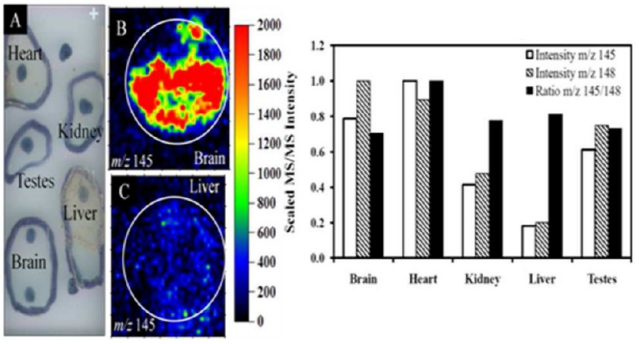

The ability of mass spectrometric imaging (MSI) techniques to generate analyte-specific distributions is improving our understanding of drug efficacy[1−4] and molecular tissue distribution.[5−8] Direct tissue analysis by matrix-assisted laser desorption (MALDI) coupled with mass spectrometry (MS) provides molecular composition analysis directly from a tissue sample. By employing multiple stages of MS, generally termed MS/MS or MS^n, analyte specificity is further enhanced and can improve drug and metabolite imaging capabilities.[4,9] Earlier imaging techniques such as magnetic resonance spectroscopy imaging[10] (MRI) or positron emission tomography[11] can be used to image a compound's distribution throughout a tissue or even a whole animal. However, these techniques lack the chemical specificity to differentiate between, for instance, a parent drug and its metabolites, because the labels attached to the drug may or may not be preserved through metabolism. This lack of chemical specificity generally necessitates further characterization, usually by tissue extraction and chromatography coupled with MS^n, ultimately resulting in nearly complete loss of spatial information. These methods can also be time-consuming and cost-prohibitive, especially when radioactive labels are employed. MSI, however, provides a label-free, direct tissue analysis of the molecular makeup of a tissue sample that can be targeted (tandem MS imaging) or untargeted (full-scan MS imaging). Both endogenous and exogenous compounds can be analyzed and compared between tissue samples, such as in comparing disease and normal states[8,12−19] or determining the distribution of pharmaceuticals.[15,17,18,20]

MALDI-based MSI does, however, have limitations. Inherently, MALDI is a poor quantitative ionization technique, although, with an appropriate internal standard, adequate quantitative results can be obtained.[9,21−26] The poor quantitative ability is generally attributed to poor ion-signal reproducibility resulting from heterogeneous matrix crystallization, sample variation, and laser energy fluctuation.[27] MALDI ion-signal variability leads to ion-signal irreproducibility in MSI applications, thus limiting the quantitative ability of MSI.

A major source of ion-signal variability is the application of the MALDI matrix.[28] Different methods of applying the matrix result in a wide variety of crystal sizes that can be larger than the laser spot size. Larger crystal sizes result in heterogeneous matrix coverage when probing on the micrometer scale. To reduce ion-signal variability, the MALDI matrix must be applied in a manner that minimizes crystal size while enhancing

extraction and cocrystallization of the target analyte from the tissue and into the matrix. To minimize crystal growth, rapidly evaporating solvents can be used; however, this can limit extraction and cocrystallization. Aside from matrix crystal variability, wide variation in tissue types can also have a major effect on the detected ion signal, especially for whole-body imaging applications. Variation between tissue types can lead to unaccountable differences in analyte extraction and ionization efficiency, leading to differences in ion signal.[17] This effect was exemplified in the MSI analysis of a whole-body sample for the distribution of administered olanzapine (OLZ) and its metabolites.[18] These experiments produced remarkable images of the distribution of OLZ-related compounds, but it was impossible to discern whether increases in MS signal directly corresponded to increases in concentration without further analysis, or what Stoeckli et al. termed "tissue-specific ionization efficiency calibration" in their discussion of ion-suppression effects in MSI.[17] Stoeckli et al. previously addressed tissue-dependent ion-signal variation in experiments by coating a solution containing the target compound over a whole-body section using a pneumatic sprayer until the tissue sample was completely wetted (and the compound was incorporated into the tissue) and then applying MSI. From the MSI data, ionization differences were determined between tissue types, and these were used to normalize images from previous experiments. Areas of ion suppression were observed and taken into account by this method; however, the application of the compound atop the tissue might not accurately reflect detection of the compound from within the tissue. These experiments did provide an excellent example of the ion-suppression effect and might lead to protocols for applications of quantitative MSI. More recently Prideaux et al. improved the technique by reproducibly spray-coating thin tissue sections with a mixture of matrix and a reference standard and then applying MS/MS imaging using multiple-reaction monitoring (MRM), which resulted in quantitative normalized images.[1] By using MRM to generate normalized images, the effect of tissue type on ion signal was taken into account; however, scan-to-scan variation in ion signal was not taken into account. Whereas the tissue is the more likely cause of significant ion-signal variation from either extraction or ionization differences, scan-by-scan variations from both laser energy fluctuations and matrix crystallization can contribute significantly to ion-signal variability, as is shown here. Another recent article by Kallback et al.[29] highlighted the importance of incorporating an internal standard for MSI quantitation through the development of novel MSI quantitation software. Their approach showed improvements in quantitation after normalization by a stable-labeled internal standard; however, for evaluating tissue-specific ionization variability, the study showed conclusive differences in ion signal detected only between areas of tissue and no tissue, not between tissue types.

An alternative to identifying tissue-specific ionization variability, as described above, would be to apply a uniform layer of a deuterated compound, to be used as an internal standard, across the MALDI target prior to placing the tissue section on the target for MSI analysis using wide-isolation MS/MS. Utilizing an internal standard in this manner has led to improved quantitative MALDI MSI on tissues and standards by generating and analyzing analyte-to-internal-standard ratio images.[1,28] Two requirements for using an internal standard in MSI are that the internal standard must be applied uniformly and the analyte and internal standard must be detected in a single analytical MS^n scan. This allows for scan-by-scan normalization of the resulting images and has been shown to significantly improve quantitation and ion-signal reproducibility.[28] Alternating MS/MS scan approaches have been shown to yield minimal improvement in ion-signal reproducibility and typically do not lead to improvements in precision for quantitation.[21] To detect both the analyte and internal standard in a single MS/MS scan, a wide-isolation or multi-isolation approach must be used.[21] Wide-isolation MS/MS is a simpler approach, typically requiring recentering and expansion of the mass-isolation window of the ion trap or lowering of the resolution of a quadrupole (for hybrid quadrupole-time-of-flight instruments). To utilize wide-isolation MS/MS, the deuterium label must be retained in the product ion. The other requirement for an internal standard is that it must be as chemically similar as possible to the target analyte, which is achieved with a deuterated internal standard.

In this study, acetyl-d_3-carnitine (AC-d_3) was utilized as an internal standard for the quantitative detection of acetyl-l-carnitine (AC) to determine concentration or distribution differences of AC in the piglet brain after treatment with a ketogenic diet. First, AC-d_3 was evaluated as an appropriate internal standard for improving MSI results using optimal cutting temperature compound (OCT), a well-known ion suppressant,[30] to generate a controlled area of ion suppression. This was followed by the quantitative analysis of AC spots beneath multiple tissue types to determine differences in detected ion signal. Finally, piglet brain tissue was analyzed by MSI for the detection of AC to determine whether analyzing the ratio of AC to AC-d_3 could account for ion suppression and improve quantitation. This article presents novel approaches for systematically evaluating and correcting for tissue-specific ion suppression, including methods for internal standard application and normalization protocols. It also highlights the benefits of this approach for both MS and MS/MS imaging applications across multiple tissue types.

MATERIALS AND METHODS

Chemicals. AC and AC-d_3 were purchased from Sigma-Aldrich (St. Louis, MO, USA). Superfrost glass plus microscope slides and HPLC-grade methanol (MeOH), ethanol (EtOH), water (H_2O), and chloroform ($CHCl_3$) were purchased from Fisher Scientific (Pittsburgh, PA, USA). Stainless steel microscope slides were purchased from Thermo Scientific (San Jose, CA, USA). Optimal cutting temperature compound (OCT) was provided by the electron microscopy laboratory at the University of Florida (Gainesville, FL, USA). Working calibration standards of AC were diluted in 50/50 MeOH/H_2O (v/v) at concentrations of 0.10, 0.20, 0.040, 0.60, 0.80, and 1.0 ng/μL. AC-d_3 was diluted in 50/50 MeOH/H_2O (v/v) at a concentration of 10 ng/μL. An Epson Stylus R280 ink-jet printer (Long Beach, CA, USA) was used to apply AC-d_3 and AC to microscope slides.[31] 2,5-Dihydroxybenzoic acid (DHB) was purchased from Acros Organics (Geel, Belgium) and prepared at a concentration of 20 mg/mL in 90/10 $CHCl_3$/EtOH (v/v).

Tissue Preparation. For analysis of AC, piglet brain tissue was provided by Dr. Peggy Borum's laboratory from the Food Science and Human Nutrition Department at the University of Florida (Gainesville, FL, USA) and was stored at −80 °C. During excision, the brain was dissected into hemispheres along the center sagittal plane and then along the coronal plane, resulting in half of a hemisphere dissected into the frontal lobe

and parietal/occipital lobe. The second cut was performed to reduce tissue sample size, allowing for simpler sectioning; coronal sections of the frontal lobe were used for analysis. Piglet brain tissue was utilized for the quantitative analysis of endogenous AC using a standard addition method. The internal standard, AC-d_3, was utilized to identify tissue-specific ionization differences. Brain, liver, testes, kidney, and heart from Sprague–Dawley rats were provided by Dr. Dieter Drexler at Bristol Meyer Squibb (Wallingford, CT, USA) and were stored at −80 °C. Transverse sections of each tissue were applied to microscope slides spotted with a mixture of AC and AC-d_3. These tissues were used to mimic a whole-body imaging experiment. One section of each tissue was placed atop a dried spot of AC/AC-d_3, and the detected AC and AC-d_3 signals were compared.

Sectioning of the tissue was performed on a Microm HM 505E cryostat (Waldorf, Germany). Tissue was sliced at −25 °C to a thickness of 20 μm and thaw-mounted onto the previously coated microscope slides. To minimize condensation, the tissue and slide were first warmed to room temperature in a vacuum desiccator for ∼30 min, and then DHB was applied with a Meinhard nebulizer (Golden, CO) at a flow rate of 2.4 mL/min.

Ion-Suppression Studies with Standards and Tissue. Prior to performing ion-suppression studies, the method of applying the internal standard was evaluated. Internal standards can be mixed with the MALDI matrix prior the matrix application step,[1] or they can be applied separately, either beneath or atop a tissue sample.[28] To evaluate these methods, 1 ng/μL of AC was applied to a microscope slide using an ink-jet printer. One milliliter of 10 ng/μL AC-d_3 was added to 10 mL of 20 mg/mL DHB and spray-coated atop the applied AC. This was compared to a glass microscope slide to which both AC and AC-d_3 had first been applied to the slide separately using an ink-jet printer, followed by spray-coating of DHB. Wide-isolation MS/MS imaging centered at m/z 205.5 ± 3 Da was performed on 2-mm squares of the applied standards. Images were then generated using the product-ion intensities of m/z 145 and m/z 148. Previous MS/MS studies using a 1-Da isolation window across the m/z range 202–209 have shown that the product ions m/z 145 and m/z 148 arise exclusively from the precursor ions m/z 204 and m/z 207, corresponding to AC and AC-d_3, respectively.

To determine whether an internal standard could identify and account for areas of ion suppression, controlled experiments mimicking areas of ion suppression were created utilizing a well-known ion suppresser, OCT;[29] even though OCT is widely recognized as an ion suppresser, we still receive tissue samples for mass spectrometric imaging that were prepared with OCT. First, 1 μL of a 1% solution of OCT was spotted onto a microscope slide, after which a 1:2 AC/AC-d_3 (v/v) mixture was added by the ink-jet printer. DHB was then applied by pneumatic spray coating, and both MS and wide-isolation MS/MS analyses were performed covering the entire OCT spot.

For multiple tissue analysis, 1-μL spots of a 1:2 AC/AC-d_3 (v/v) mixture was applied atop a microscope slide. Brain, liver, testes, kidney, and heart sections were each placed over one of the spots. One spot was left uncovered and analyzed to determine the detected m/z 145/148 ratio. DHB was spray-coated over the entire slide, and each tissue was analyzed by wide-isolation MS/MS.

Finally, the distribution of AC was determined in a coronal section of piglet brain tissue. Calibration standards of AC were first applied to a glass slide (1 μL) with a micropipet and allowed to dry. AC-d_3 was then applied covering the entire slide with an ink-jet printer. Coronal sections of piglet brain tissue were then sectioned to 20 μm and thaw-mounted atop the calibration standards.

Instrumentation. All experiments evaluating ion suppression were performed on a MALDI LTQ XL instrument equipped with a 60-Hz, 337-nm nitrogen laser with a spot size of 100 μm (Thermo Corporation, San Jose, CA, USA). For MS/MS imaging experiments on the LTQ instrument, a 6-Da wide-isolation window was centered at m/z 205.5. The $[M + H]^+$ ions of the compounds were fragmented using collision-induced dissociation, and the product ions of the compounds were monitored: for AC, m/z 204 → 145; AC-d_3, m/z 207 → 148. Sample slides were inserted into the vacuum chamber and rastered beneath the laser at a step size of 100 μm. Data and images from the LTQ instrument were processed with Qual Browser (Thermo Scientific) and Surfer 8 (Golden Software, Golden, CO, USA). Normalized images from the LTQ instrument were generated in Surfer 8 from extracted data. For ion-suppression determinations, the product-ion intensities of m/z 145 and m/z 148 and the ratio of m/z 145/148 were analyzed.

MSI experiments of AC in piglet brain tissue were performed with a Synapt MALDI-Q-Ion Mobility (T-wave cell) time-of-flight (Q-TOF) instrument equipped with a 200-Hz, 355-nm YAG laser with a spot diameter of 150 μm (Waters Corporation, Milford, MA, USA) in full-scan MS mode. Resulting data from the Q-TOF instrument were processed using BioMap (Novartis, Basel, Switzerland). BioMap was utilized to generate analyte-to-internal-standard normalized images with the "divide" function built into the software. For quantitative determinations of endogenous AC, regions of interest were generated covering the calibration standards and a standard addition analysis was performed using the signal from the spotted calibration standards and the uniformly applied internal standard. As in any experiments that employ human specimens, appropriate blood-borne pathogen safety precautions should be followed. Also, application of matrix solutions should be performed in a hood.

RESULTS AND DISCUSSION

Internal Standard Application. Prior to evaluating tissue-dependent ion-signal variation, methods for the application of the internal standard AC-d_3 were evaluated. It has previously been shown that scan-by-scan normalization with wide-isolation MS/MS spectra of AC by AC-d_3 results in a significant improvement in ion-signal reproducibility, calibration curve linearity and image quality.[21,28] To evaluate the addition of AC-d_3 for imaging studies, AC-d_3 was applied both mixed with the matrix and separately from the matrix. Wide-isolation MS/MS was performed over a 10 × 10 raster step square (100 scans with a 200-μm step size) on the applied standards. For normalized images, the intensity of m/z 145 was divided by the intensity of m/z 148 for each MS/MS scan. The mean-centered results are plotted in Figure 1. Panels A–C of Figure 1 show plots of the ion-intensity images generated from m/z 145, m/z 148, and m/z 145/148, respectively, upon application of the AC-d_3 mixed with the matrix. The relative standard deviation (RSD) in product-ion intensity was 57% for m/z 145, 54% for m/z 148, and 60% for m/z 145/148. The lack of improvement

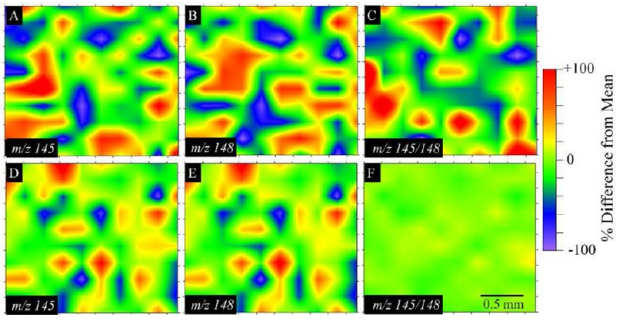

Figure 1. MS/MS images comparing two methods for applying the internal standard AC-d_3. (A–C) AC-d_3 was mixed with the MALDI matrix solution and spray-coated atop AC, which was applied with an ink-jet printer. (D–F) Alternatively, AC and AC-d_3 were applied separately with the ink-jet printer and then the MALDI matrix solution was spray-coated on top. Images were generated from the intensity of the product ions (A,D) m/z 145 or (B,E) m/z 148 or (C,F) by normalizing the intensity of m/z 145 to m/z 148 at each raster step. The intensities are mean-centered. Thus, the average intensity is 0% difference, and the intensities vary from −100% (zero absolute intensity) to +100% (2 times the average intensity).

in image quality and signal variation indicates that application of an internal standard with the matrix does not lead to improved analytical performance. This might be due to differences in cocrystallization between AC and AC-d_3 with DHB. Panels D–F of Figure 1 show plots of the ion-intensity images generated from m/z 145, m/z 148, and m/z 145/148, respectively, when AC-d_3 was applied separately from the matrix and AC. The signal intensity patterns in Figure 1D,E are similar to each other, indicating that AC and AC-d_3 behave similarly in ionization and cocrystallization. The normalized m/z 145/148 image in Figure 1F shows a relatively uniform ion image and better represents the distribution of AC over the given area. The RSD in product-ion intensity was 42% for m/z 145, 41% for m/z 148, and 8% for m/z 145/148, indicating that the application of the internal standard separately from the matrix solution was superior. Both AC and AC-d_3 appear to cocrystallize with the matrix in a similar manner, as indicated by the similar pattern observed in Figure 1D,E. It is unlikely that the pattern was replicated by the ink-jet printer multiple times; it is more likely due to differences in the crystallization of DHB. From these results, it was concluded that the internal standard would be added separately from the MALDI matrix for all further experiments.

Ion Suppression with Standards. To determine whether an internal standard could help identify and account for areas of ion suppression, analysis of AC and AC-d_3 was performed using OCT as an ion suppressant. MSI was performed over spots of applied OCT (1 mm across) and AC and AC-d_3 (each ∼3 mm across) in MS and wide-isolation MS/MS mode. Images from the MSI experiments with MS are shown in Figure 2. Three methods of image normalization reported in the literature were compared, including normalizing the analyte signal to the matrix signal, the analyte signal to the total ion current (TIC) at each spot, and the analyte signal to an externally applied internal standard.[31] Un-normalized images are shown in Figure 2A–C. Normalized images are shown in Figure 2D–F. The area of the spotted OCT is clearly visible from plotting m/z 332, which corresponds to the OCT additive benzylalkonium chloride (Figure 2A). Areas of ion suppression resulting from OCT are shown in the MS images of AC and AC-d_3 (Figure

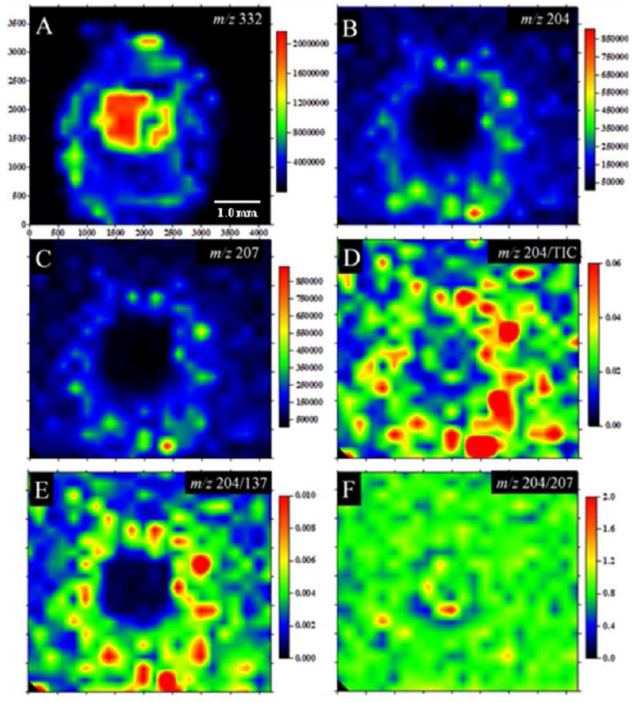

Figure 2. MS images of AC mixed with AC-d_3 (each ∼3 mm across) applied atop a spot of dried OCT (∼2 mm across). The resulting MS images show (A) the distribution of OCT resulting in ion suppression, visible in MS images for (B) AC and (C) AC-d_3. (D–F) Comaprison of multiple methods of normalization. The MS image for AC should appear uniform resulting for the uniform application. This is produced only by normalizing to the internal standard. The color scales for A–C were determined from the plotted ion-intensity values. The color scales for D–F were determined from the intensity ratio of m/z 204 to the respective value.

2B,C). Both AC and AC-d_3 were applied atop the slide homogeneously with an ink-jet printer, which should lead to uniform signal distribution throughout the area analyzed; however, the presence of OCT results in drastic signal reduction. Without prior knowledge of ion suppression, one may conclude an uneven distribution of AC using the ion intensity alone. These areas of ion suppression are not identified (nor corrected for) when performing signal normalization of the AC ion (m/z 204) to the TIC (Figure 2D) or to the major MALDI matrix ion (m/z 137) (Figure 2E). These normalization methods still produce images showing uneven AC signal distribution, although normalization by the TIC is more successful than is normalizing by the matrix. Normalizing to AC-d_3, however, does result in an image showing nearly uniform distribution of AC; this demonstrates that normalizing to the internal standard (which has chemical properties nearly identical to those of the target analyte) can successfully correct for ion suppression.

Tissue-Specific Signal Variability. To test whether normalizing images by an internal standard can be used with tissue analysis to identify tissue-specific ion suppression, multiple tissue types were sectioned and applied atop a pipetted spot of a 1:2 mixture of AC and AC-d_3. Shown in Figure 3A is a photograph of the slide with tissues outlined and identified. A black spot was applied to the backside of the slide to mark where the spots of AC/AC-d_3 were applied. For analysis by wide-isolation MSI, a rectangle was drawn surround the applied AC/AC-d_3 and analyzed using a 100-μm step size.

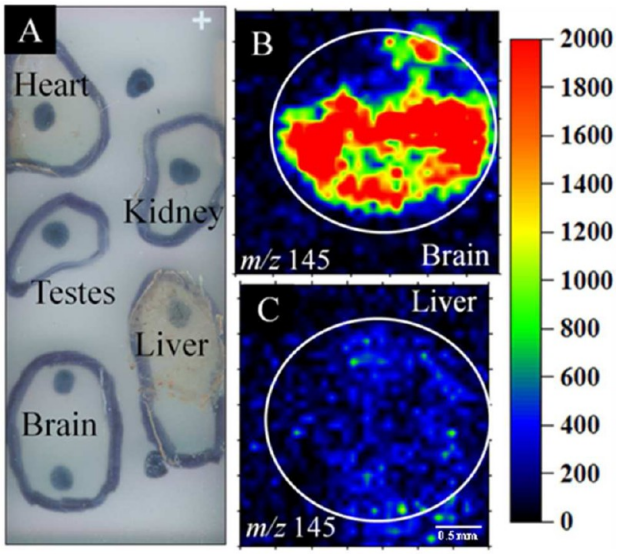

Figure 3. Multiple tissue analysis of AC ion-signal variability using wide-isolation MS/MS. (A) Optical image of the glass slide with multiple tissue sections applied over spots of 1:2 mixture of AC/AC-d_3 (marked with black spots). (B) MS/MS image of product ion for AC applied under the brain section compared to (C) MS/MS image from the liver tissue. The detected signal for AC was decreased by 90% from brain to liver tissue. The intensity scale reflects absolute counts of m/z 145.

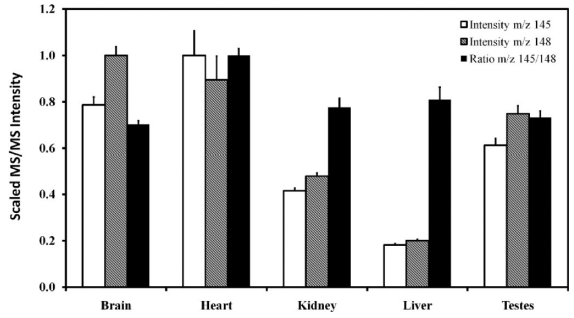

Figure 4. Wide-isolation MS/MS data were collected from one spot of AC and AC-d_3 spotted beneath one section of multiple tissue types. Ion intensities were summed corresponding to the spotted standards beneath each tissue. Error bars represent standard deviations of the mean. MS/MS intensities of m/z 145 and m/z 148 were summed over the raster area, and these intensities (or the ratio) were scaled as a percentage of the maximum intensity. A significant decrease in ion signal is observed for both the AC and AC-d_3 in the kidney and liver sections compared to the brain, heart, and testes. However, the ratio of AC to AC-d_3 remains constant, varying by only 13% RSD among the five tissue types, whereas the AC and AC-d_3 intensities vary by 70% RSD among tissue types.

The resulting data were extracted into Excel for ratio determination, and Surfer 8 was used to produce the MS/MS images. MS/MS images of AC from the spots applied beneath the brain and liver sections are shown in panels B and C, respectively, of Figure 3. The ion intensity of m/z 145 showed a 90% reduction in the liver section compared to the brain section. This signal reduction could result from inefficient extraction, poor cocrystallization into the matrix, or from ion suppression from an endogenous compound in the liver tissue; however, it is not possible to determine which effect was dominant.

A summary of the analysis of all of the tissues is shown in Figure 4, which presents a plot of the summed intensities covering the entire AC/AC-d_3 spot. The intensities were summed to minimize the effect of MS/MS scan in which little or no ion intensity was measured, which can happen occasionally when performing MS/MS experiments directly from nonuniform tissue samples. The histogram was scaled to the maximum signal or ratio detected across the tissue types for ease of comparison. Significant tissue-specific signal attenuation is observed in both the liver and kidney, as well as slightly in the testes. Analyzing the data using only the ion intensity would lead to an incorrect conclusion that there were a lower concentration of AC in these tissues. After scan-by-scan normalization with the AC-d_3 internal standard, the ratios of the detected AC/AC-d_3 were within ±13% from tissue to tissue. Clearly, use of an isotopically labeled internal standard is critical for a comparison of the endogenous concentration of AC between tissue types.

In addition to known instances of ion suppression or tissue-specific signal variation, ion suppression was also observed in experiments designed to quantify AC in a coronal section of piglet brain tissue. Although initially not intended for this study, this approach with the Q-TOF instrument clearly demonstrates the necessity of applying an appropriate internal standard for any quantitative estimation. Shown in Figure 5A is the MS intensity of m/z 204 corresponding to the molecular ion of AC. A clear decrease in the AC signal is observed in the white matter compared to the gray matter. Calibration spots were applied beneath the tissue section and are also visible in the MS image in Figure 5A. Figure 5B is the MS image of m/z 207 from the AC-d_3 internal standard, which was uniformly applied beneath the tissue by an ink-jet printer. A distinct reduction in the AC-d_3 signal is also observed in the white matter compared to the gray matter, even though AC-d_3 was applied uniformly. White and gray matter were identified by generating images of lipids that have been previously shown to localize between the two tissue types.[33] This suggests that the difference in the AC signal observed in Figure 5A might reflect not differences in the AC concentration but rather variations in either extraction or ionization efficiency between white and gray matter. Analysis of the AC/AC-d_3 ratio (Figure 5C) gives a better indication of the distribution of AC between gray and white matter in this sample by accounting for spot-to-spot signal variation and, more importantly, for ionization variability and extraction differences. In this example, we used MS rather than MS/MS and thus relied on the increased mass resolution of the Q-TOF instrument for identification of AC and AC-d_3. To minimize the risk of interfering ions, spectra were binned to 0.1 Da for both AC and AC-d_3; we would predict that any significant interference would be reflected in the error in the calibration curve. Furthermore, comparison of the calibration curves generated from the MSI experiments (Figure 5D,E) show a dramatic improvement in linearity and precision when scan-by-scan normalization to the deuterated internal standard was performed. Also noteworthy in these experiments is the limited dynamic range in the calibration curve. In this example, only six calibration spots were applied in this tissue section because of space limitations when applying multiple calibration spots beneath the tissue. The calibration curve was expanded both below 50 $\mu g/g_{tissue}$ and above 460 $\mu g/g_{tissue}$ by applying lower and higher calibration spots beneath serial tissue sections; however, extending the calibration curve with data from multiple tissue sections resulted in poor calibration. This

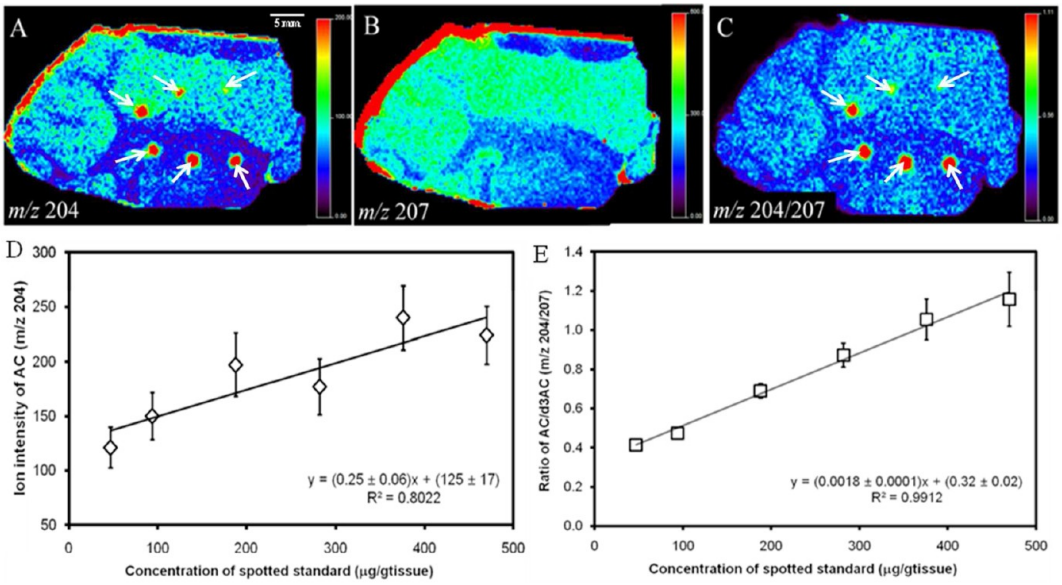

Figure 5. MS image of piglet brain tissue for the detection of endogenous AC. (A) Image of the $[M + H]^+$ ion corresponding to AC (m/z 204) shows a clear differentiation between white and gray matter of the brain. (B) Applied AC-d_3 shows a similar pattern, implying that there is either decreased extraction or ionization from the two tissue types. (C) Ratio image of AC/AC-d_3 results in a better representation of the distribution of AC within the brain sample while improving the linearity of calibration curve. Calibration curves plotted with (D) the ion intensity of m/z 204 versus (E) the ratio of m/z 204/207. The appearance of saturated calibration spots are graphical due to scaling to show the endogenous levels of AC.

demonstrated the advantage of generating all of the calibration curve data from a single tissue section. In this case, the endogenous concentration of AC observed in the tissue falls well within the calibration range of 50−460 $\mu g/g_{tissue}$.

Although it is not possible to determine which factor, extraction or ionization, is the dominant source of signal variation, it could well be a combination of the two. For protein analysis, multiple washing steps are routinely performed to remove the majority of the lipids prior to MSI, because they tend to suppress protein ion signals. Such washes are not typically performed for small-molecule MSI because of the solubility of small molecules in washing solutions, which might result in analyte migration or loss. Differences in the amount of lipids in various tissue types as well as within a single tissue type might also create significant differences in the extractability of a particular compound. The extraction can be optimized for a particular tissue type; however, even in a single tissue such as brain (Figure 5), there can be regional variations, as between gray and white matter. A single tissue type can vary significantly on the millimeter scale, and across multiple tissue types, these effects can be exacerbated. Applying an internal standard, preferably a deuterated analogue, can help control for these extraction and ionization issues that otherwise limit the potential for quantitative MSI.

CONCLUSIONS

These results demonstrate that performing an MSI experiment without an internal standard can lead to inaccurate conclusions about individual compound's distribution within a tissue and more so across multiple tissue types, such as in a whole-body MSI experiment. Applying an internal standard corrects for tissue-specific signal variability resulting from either ion suppression or analyte extraction. The methods developed here overcome these tissue-specific variations, leading to more conclusive results about concentration differences in a given sample. The ability to quantitatively map a drug's time-resolved distribution throughout an organ or entire animal could provide invaluable information about a drug's efficacy. Unique determinations could also be made about a drug's distribution, as well as any changes these compounds are inducing on the endogenous compounds present in the sample, such as metabolites, lipids, and proteins.

AUTHOR INFORMATION

Corresponding Author

*E-mail: ryost@ufl.edu. Phone: (352)392-0557. Fax: (352) 392-4651.

Notes

The authors declare no competing financial interest.

ACKNOWLEDGMENTS

The authors thank Dr. Peggy Borum from the Food Science and Human Nutrition Department at the University of Florida for providing the piglet brain tissue and Dr. Dieter Drexler at Bristol Meyer Squibb (Wallingford, CT) for providing the brain, liver, testes, kidney, and heart from Sprague−Dawley rats. We also acknowledge partial funding from National Science Foundation Grant PIRE-0730072 and from Thermo Scientific.

REFERENCES

(1) Prideaux, B.; Dartois, V.; Staab, D.; Weiner, D. M.; Goh, A.; Via, L. E.; Barry, C. E., 3rd; Stoeckli, M. *Anal. Chem.* **2011**, *83*, 2112−2118.

(2) Wiseman, J. M.; Ifa, D. R.; Zhu, Y.; Kissinger, C. B.; Manicke, N. E.; Kissinger, P. T.; Cooks, R. G. *Proc. Natl. Acad. Sci. U.S.A.* **2008**, *105*, 18120−18125.

(3) Nilsson, A.; Fehniger, T. E.; Gustavsson, L.; Andersson, M.; Kenne, K.; Marko-Varga, G.; Andren, P. E. *PLoS One* **2010**, *5*, e11411.

(4) Drexler, D. M.; Garrett, T. J.; Cantone, J. L.; Diters, R. W.; Mitroka, J. G.; Prieto Conaway, M. C.; Adams, S. P.; Yost, R. A.; Sanders, M. *J. Pharmacol. Toxicol. Methods* **2007**, *55*, 279−288.

(5) McDonnell, L. A.; Corthals, G. L.; Willems, S. M.; van Remoortere, A.; van Zeijl, R. J.; Deelder, A. M. *J. Proteomics* **2010**, *73*, 1921−1944.
(6) Nemes, P.; Woods, A. S.; Vertes, A. *Anal. Chem.* **2010**, *82*, 982−988.
(7) Landgraf, R. R.; Prieto Conaway, M. C.; Garrett, T. J.; Stacpoole, P. W.; Yost, R. A. *Anal. Chem.* **2009**, *81*, 8488−8495.
(8) Garrett, T. J.; Prieto-Conaway, M. C.; Kovtoun, V.; Bui, H.; Izgarian, N.; Stafford, G.; Yost, R. A. *Int. J. Mass Spectrom.* **2007**, *260*, 166−176.
(9) Koeniger, S. L.; Talaty, N.; Luo, Y.; Ready, D.; Voorbach, M.; Seifert, T.; Cepa, S.; Fagerland, J. A.; Bouska, J.; Buck, W.; Johnson, R. W.; Spanton, S. *Rapid Commun. Mass Spectrom.* **2011**, *25*, 503−510.
(10) Beckmann, N.; Laurent, D.; Tigani, B.; Panizzutti, R.; Rudin, M. *Drug Discov. Today.* **2004**, *9*, 35−42.
(11) Kuratsune, H.; Watanabe, Y.; Yamaguti, K.; Jacobsson, G.; Takahashi, M.; Machii, T.; Onoe, H.; Onoe, K.; Matsumura, K.; Valind, S.; Kitani, T.; Langstrom, B. *Biochem. Biophys. Res. Commun.* **1997**, *231*, 488−493.
(12) Shimma, S.; Sugiura, Y.; Hayasaka, T.; Hoshikawa, Y.; Noda, T.; Setou, M. *J. Chromatogr. BLife. Sci.* **2007**, *855*, 98−103.
(13) Cornett, D. S.; Frappier, S. L.; Caprioli, R. M. *Anal. Chem.* **2008**, *80*, 5648−5653.
(14) Caprioli, R. M.; Farmer, T. B.; Gile, J. *Anal. Chem.* **1997**, *69*, 4751−4760.
(15) Hsieh, Y.; Chen, J.; Korfmacher, W. A. *J. Pharmacol. Toxicol. Methods* **2007**, *55*, 193−200.
(16) Reyzer, M. L.; Caprioli, R. M. *Curr. Opin. Chem. Biol.* **2007**, *11*, 29−35.
(17) Stoeckli, M.; Staab, D.; Schweitzer, A. *Int. J. Mass Spectrom.* **2007**, *260*, 195−202.
(18) Khatib-Shahidi, S.; Andersson, M.; Herman, J. L.; Gillespie, T. A.; Caprioli, R. M. *Anal. Chem.* **2006**, *78*, 6448−6456.
(19) Landgraf, R. R.; Garrett, T. J.; Calcutt, N. A.; Stacpoole, P. W.; Yost, R. A. *Anal. Chem.* **2007**, *79*, 8170−8175.
(20) Signor, L.; Varesio, E.; Staack, R. F.; Starke, V.; Richter, W. F.; Hopfgartner, G. *J. Mass Spectrom.* **2007**, *42*, 900−909.
(21) Reich, R. F.; Cudzilo, K.; Levisky, J. A.; Yost, R. A. *J. Am. Soc. Mass Spectrom.* **2010**, *21*, 564−571.
(22) Bucknall, M.; Fung, K. Y.; Duncan, M. W. *J. Am. Soc. Mass Spectrom.* **2002**, *13*, 1015−1027.
(23) Sleno, L.; Volmer, D. A. *Rapid Commun. Mass Spectrom.* **2005**, *19*, 1928−1936.
(24) Hatsis, P.; Brombacher, S.; Corr, J.; Kovarik, P.; Volmer, D. A. *Rapid Commun. Mass Spectrom.* **2003**, *17*, 2303−2309.
(25) Hankin, J. A.; Murphy, R. C. *Anal. Chem.* **2010**, *82*, 8476−8484.
(26) Pirman, D. A.; Reich, R. F.; Kiss, A.; Heeren, R. M. A.; Yost, R. A. *Anal. Chem.* **2012**, http://dx.doi.org/10.1021/ac302960j.
(27) Gusev, A. I.; Wilkinson, W. R.; Proctor, A.; Hercules, D. M. *Anal. Chem.* **1995**, *67*, 1034.
(28) Pirman, D. A.; Yost, R. A. *Anal. Chem.* **2011**, *83*, 8575−8581.
(29) Källback, P.; Shariatgorji, M.; Nilsson, A.; Andrén, P. E. *J. Proteomics* **2012**, *75*, 4941−4951.
(30) Schwartz, S. A.; Reyzer, M. L.; Caprioli, R. M. *J. Mass Spectrom.* **2003**, *38*, 699−708.
(31) Baluya, D. L.; Garrett, T. J.; Yost, R. A. *Anal. Chem.* **2007**, *79*, 6862−6867.
(32) Naofumi, H.; Yuki, S.; Mitsutoshi, S. *J. Mass Spectrom. Soc. Jpn.* **2008**, *56*, 77.
(33) Trim, P. J.; Atkinson, S. J.; Princivalle, A. P.; Marshall, P. S.; West, A.; Clench, M. R. *Rapid Commun. Mass Spectrom.* **2008**, *22*, 1503−1509.